

Effects of Background Noise on Speech Intelligibility for Hidden Hearing Loss Sufferers:
“The Cocktail-Party Effect”

A THESIS

Submitted to the Faculty of
The University of Michigan in partial fulfillment
of the requirements
for the Honors degree of Bachelor of Science

by

Jonah Lindau

The University of Michigan

Ann Arbor, MI

March 2023

Abstract

Hidden Hearing Loss (HHL) is a binaural processing deficit characterized by the difficulties it presents with sound localization despite audiometric thresholds remaining unaffected. HHL is caused by neuropathies of the spiral ganglion neuron (SGN)—inner hair cell (IHC) complex consisting of myelin sheath degradation (myelinopathy) of the unmyelinated segment of the SGN adjacent to the IHC synapse and loss of IHC synapse (synaptopathy). These neuropathies are thought to be caused by aging, overexposure to loud noises, and other demyelinating diseases. People suffering from HHL may find speech intelligibility notably difficult in noisy environments as a result of sound localization deficits. This has been coined the “Cocktail-Party Effect.” This study investigated the cocktail-party effect by simulating responses of SGN fibers of varying myelinopathy severity to white noise-disrupted sound stimuli. Simulations were conducted using a series of models including an acclaimed peripheral auditory system model outputting auditory nerve (AN) spike probabilities, an SGN fiber model using the NEURON software, and a previously developed SGN neuropathy model used to implement the effects of myelinopathy and output AN spike times. Results indicated an increase in amplitude of SGN fiber population activity with increasing white noise sound level. Increases in myelinopathy as well as frequency of sound signal delivered increases in compound action potential (CAP) delay. Comparing CAP changes with respect to frequency showed frequency dependent changes for delay, peak amplitude, and CAP width.

Chapters	Page
Abstract	2
Introduction	4
Methodology	7
Peripheral Auditory System Model (Meddis Model).....	7
Development of AWGN Sound Signal.....	7
Implementation of AWGN Sound Signal into Meddis Model.....	9
SGN Fiber Model.....	12
Generating AN Spike Times.....	14
Results and Discussion	17
Effects of myelinopathy on SGN response to AWGN sound.....	17
Comparison of frequency impact on SGN activation patterns.....	23
Limitations.....	25
Further research.....	26
References	27
Acknowledgements	29

Introduction

Sound localization is imperative for the survival of animals in the wild – both predators (to locate prey) and prey (to avoid becoming a meal). This ability allows mammals to estimate the source of a sound from sound signals too brief to be tracked or scanned (Heffner et al., 1992). Sound localization is performed binaurally (meaning a response from each ear) in the Superior Olivary Complex (SOC) from the Spiral Ganglion Neurons (SGNs) to the Medial Superior Olives (MSOs). When a sound signal is emitted on the azimuthal plane, it reaches each ear of a listener at different times (Budak et al., 2022). Although minuscule, this time delay between the sound signal reaching the right ear vs. the left ear allows for sound localization. When a signal reaches the inner hair cells (IHCs) of each ear, a signal is propagated to the SGNs, initiating the SOC pathway. Following the excitation of the IHCs from the sound signal, SGNs from each ear, located in the ear's cochlea, are excited and fire signals to both the SGNs and the GBCs located in the cochlear nucleus. The MSOs are able to calculate the location of a sound by measuring a time delay between series of excitatory and inhibitory stimuli provided by Spherical Bushy Cells (SBCs) and Globular Bushy Cells (GBCs) respectively. Each of the SBCs and GBCs send signals to both ipsi- and contralateral MSOs. The MSOs will only fire if they receive excitatory and inhibitory signals from both the ipsi- and contralateral SBCs. The MSOs measure the latency between excitation and inhibition as well as difference signal intensity to calculate the azimuthal angle corresponding to the origin of the sound stimulus. This method is successful at pinpointing sound stimulus origin within a few degrees (Budak et al., 2022).

Due to the nature of binaural excitatory input function, the signal emitted from the sound stimulus reaching the contralateral ear must reach the MSO before that of the ipsilateral ear. This time difference between the arrival of a sound stimulus to each ear is called the interaural time

difference (ITD). This compensates for the internal delay caused by the longer neural path (Budak et al., 2022). The ITDs corresponding to the highest activity in an MSO are called the best ITDs and occur from contralateral-favoring sound stimulus origins (Harper and McAlpine, 2004). The ability to resolve these time differences for sound localization is very precise and can be easily influenced by the infrastructure of the pathway. Therefore any damage or irregularities along the pathway will greatly inhibit sound localization. These irregularities present themselves in deviations in compound action potentials (CAP) from those of normal audiometric thresholds including reduction of CAP amplitude, increase in latency, and increase in CAP width (Budak et al., 2021; Budak et al., 2022).

In an undamaged human brain, sound localization contributes greatly to speech intelligibility. Hidden Hearing Loss (HHL) is a binaural hearing deficit characterized by difficulties presented with speech intelligibility in noisy environments (Kohrman et al., 2020). The ability to use sound localization in noisy environments to eliminate background noise and focus on one sound source has been coined, the “cocktail-party effect.” To a person without HHL, speech intelligibility in a conversation should be relatively consistent regardless of the presence of background noise or lack thereof. One suffering from HHL however, will find speech intelligibility significantly more difficult in the presence of background noise, despite maintaining normal audiometric thresholds in the brain. This condition has been shown to be caused by the degradation of myelin (myelinopathy) and degradation of synapses (synaptopathy) on the type I cochlear SGNs adjacent to IHCs. These deficits have been found to cause reduced amplitudes in sound-evoked auditory nerve (AN) CAPs as well as marginal CAP latencies due to myelinopathy (Budak et al., 2021). There have been indications of neuropathy onset due to moderate noise exposure, aging, and other demyelinating diseases such as Gaullian-Barré

Syndrome (Wan and Corfas, 2017). Synaptopathy and myelinopathy also disrupt signal propagation from the SBCs to the MSOs affecting ITDs and eliminating signals (Budak et al., 2022). These consequences result in a decrease in MSO activity causing miscalculations in sound localization, hence the “cocktail-party effect.” In this study, we test the cocktail-party effect by simulating the effects of background noise over an intended sound signal (representative of speech) on CAP times and amplitude in both healthy and HHL suffering brains. We hypothesize that increased levels of background noise will deplete CAP amplitude and increase CAP latency as severity of myelinopathy increases. For the purpose of this experiment, we focused solely on myelinopathy, specifically demyelination contributing to the length of the unmyelinated segment (L_u) at the beginning of the IHC adjacent end of the SGN. To test this hypothesis, we modified computational models from Budak et al. (2021) and Budak et al. (2022) as well as an acclaimed model of cochlear sound processing (Meddis et al., 2013) to simulate type I SGN fiber responses to sound stimuli in added white gaussian noise (AWGN) with SGN unmyelinated segments of random lengths between 10 and 20 μM . These simulations were run with IHCs with varying thresholds (dependent on magnitude of the incoming sound stimulus) and their channels of varying best frequencies (BF; determined using the Greenwood function). Best frequencies are characteristic for each channel and represent the frequency at which a given channel will respond best at a given sound level.

Model results indicated an increase in peak amplitude of the cumulative activity of SGN fiber populations with an increase in background noise. Results also showed an increase in CAP width with increasing myelinopathy. SGN response delays increased with increasing myelinopathy.

CAP results were compared with respect to frequency by comparing the ratio of parameter difference (between normal and HHL values) by the parameter's normal values (as opposed to HHL values) with a sound signal of 70dB SPL. Results showed the ratio of difference in peak amplitude to the normal peak amplitude increased with increasing frequency for all noise levels. We also found that the ratio of difference in width to the normal width reached a minimum at the moderate frequency, increasing when frequency diverged from the moderate frequency. Finally, the ratio of difference in delay showed varying behaviors depending on noise SPL.

Methodology

Peripheral Auditory System Model (Meddis Model)

Development of AWGN Sound Signal

The Meddis model (Meddis et al., 2013) was a previously developed computational model of the peripheral auditory system of a guinea pig. Guinea pigs were chosen in the making of this model due to their characteristic ability to detect sound frequencies much closer to the human frequency range than a rat or mouse is able to. This model constructs a series of 21 channels of varying “best-frequencies” (BFs) using the Greenwood function – a cochlear frequency-position function based on physiological data (Greenwood, 1990). BFs are calculated within bounds that are determined by the frequency range a guinea pig can hear. In the Meddis model, this range used was 5.6kHz–32kHz. Since we wanted to create a human model, we simply changed this range to 1kHz-8kHz, slightly larger than the common range for human speech (Salmon et al., 2023). We included three types of IHC-SGN synapses depending on responses due to varying sound levels to end up with 21 channels each of high threshold (HT),

medium threshold (MT), and low threshold (LT) channels. Channels of different thresholds will have different spontaneous firing rates with HT channels having the lowest spontaneous firing rates and LT channels having the greatest spontaneous firing rates.

To run a simulation, a sound wave characterized by frequency and sound pressure level (dB SPL) must be input. We picked three frequencies within the range of BFs previously calculated to test response to low, medium, and high frequencies: 1966Hz, 4920Hz, and 7265Hz. Since this experiment investigates a sound wave in noise, a disruptive signal was implemented over the original sound wave to represent speech-in-noise. The AWGN (added white gaussian noise) MATLAB function implements a scaled white gaussian noise signal which can be specified by setting a seed. To make this simulation as realistic as possible, the sound stimulus input begins with a 1ms “dead-zone” buffer followed by 2.5ms of white-noise alone, then an implementation of the sound curve into the white noise for another 2.5ms, concluding with another 1ms “dead-zone” buffer to ensure all SGN responses are recorded. This simulates a noisy room with speech then introduced – the exact scenario found in the case of the “cocktail-party effect.” To build this simulation, the AWGN function was used over a 0dB sound (flat-line at 0) resulting in a white gaussian noise signal. This noise signal was then scaled to each of 0dB, 30dB, 50dB, and 70dB using the “setleveldb” function. Sound curves representing speech at each frequency previously mentioned were scaled to each of 30dB, 50dB, and 70dB. Each white noise signal was then summed with each sound signal to represent the speech-in-noise effectively producing a sound-to-noise ratio (SNR),

$$SNR = \frac{dB_{sound}}{dB_{noise}}. \quad (1)$$

Figure 1 shows an example sound curve fed into the Meddis Model. This concludes the construction of the AWGN sound signals.

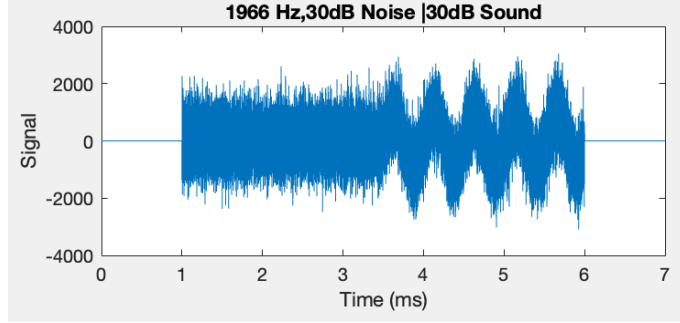


Figure 1: Sound curve used in running the Meddis Model. A 30dB white noise runs for 2.5ms starting at $t = 1\text{ms}$. At 3.5ms , the 30dB sound signal is introduced and continues for another 2.5ms until it stops at 6ms . The sound curve begins and concludes with a 1ms “dead-zone” buffer to ensure all SGN activity is recorded in future steps.

Implementation of AWGN Sound Signal into Meddis Model

The Meddis Model (Meddis, 2011) takes an input sound stimulus and simulates responses from the middle ear to the SGNs. The model begins with a sound pressure wave into the external ear which outputs the original sound pressure wave with an added resonance. Next, the stapes response is measured with live-human patient models from Huber (2001). The stapes response intakes the output sound pressure at the tympanic membrane (TM). The response is calculated as the stapes displacement (in meters) in response to frequencies above 1kHz

$$d = \frac{v}{2\pi f} = \frac{kp}{2\pi f} \quad (2)$$

where v is the stapes velocity, f is the sound signal frequency, k is a constant, and p is sound pressure. The acoustic reflex acts as a moderator for the stapes in the presence of a loud sound. This is modeled as a negative feedback loop.

The basilar membrane (BM) is modeled using a “Dual-Resonance-Non-Linear” (DRNL) filter architecture (Lopez-Poveda and Meddis, 2001). The BM model uses the BFs found using the Greenwood function previously and is modeled at discrete locations defined by the BF values. The BM displacement, $disp$, is used to then calculate IHC stereocilia displacement, $u(t)$

$$\tau_c \frac{du(t)}{dt} + u(t) = \tau_c C_{cilia} disp_t \quad (3)$$

where C_{cilia} is a gain factor converting BM displacement $disp_t$ to cilia displacement $u(t)$ and τ_c is a time constant for cilia displacement.

With the cilia displacement, the apical conductance $G(u)$ can then be calculated

$$G(u) = G_{cilia}^{max} \left[1 + \exp\left(-\frac{u(t)-u_0}{s_0}\right) \left[1 + \exp\left(-\frac{u(t)-u_1}{s_1}\right) \right]^{-1} + G_a \right] \quad (4)$$

where G_{cilia}^{max} is conductance when all transduction channels are open and G_a is the passive conductance of the apical membrane. u_0 , s_0 , u_1 , and s_1 are all constants describing the proportion of open channels.

The model then calculates the membrane potential, $V(t)$, of the cell body as

$$C_m \frac{dV(t)}{dt} + G(u)(V(t) - E_t) + G_k(V(t) - E'_k) = 0 \quad (5)$$

where C_m is the cell capacitance, G_k is the fixed membrane conductance, E_t is the endocochlear potential, and E'_k is the resistance corrected reversal potential of the basal current E_k for

$$E'_k = E_k + E_t R_{pc} \quad (6)$$

where R_{pc} is the resistance of the supporting cells. The membrane potential $V(t)$ describes the depolarization event opening of calcium channels, changing the calcium current, I_{Ca} ,

$$I_{Ca}(t) = G_{Ca}^{max} m_{I_{Ca}}^3(t)(V(t) - E_{Ca}) \quad (7)$$

where E_{Ca} is the reversal potential of calcium and G_{Ca}^{max} is the calcium conductance near the synapse-adjacent open channels.

$m_{ica}(t)$ is the fraction of open calcium channels with steady state $m_{I_{ca,\infty}}$ modeled by a Boltzmann function,

$$m_{I_{ca,\infty}} = \left[1 + \beta_{ca}^{-1} \exp(-\gamma_{ca} V(t)) \right]^{-1} \quad (8)$$

where γ_{ca} and β_{ca} are constants chosen to make the result comparable to experimental observations of calcium currents. $m_{ica}(t)$ previously described is modeled by

$$\tau_m \frac{dm_{I_{ca}}(t)}{dt} + m_{I_{ca}}(t) = m_{I_{ca,\infty}} \quad (9)$$

where τ_m is a time constant for the calcium current. $I_{ca}(t)$, a function of calcium current, can model presynaptic calcium concentration, $[Ca^{2+}](t)$,

$$\frac{d[Ca^{2+}](t)}{dt} = I_{ca}(t) - \frac{[Ca^{2+}](t)}{\tau_{[Ca]}}, \quad (10)$$

where $\tau_{[Ca]}$ is a time constant reflecting the amount time presynaptic calcium lingers near the synapse. This constant accounts for the rate at which calcium clears from the synapse-adjacent region. This effectively determines the degree of spontaneous firing of the synapse where low $\tau_{[Ca]}$ values indicate low spontaneous rate (LSR) synapses and high $\tau_{[Ca]}$ values indicate high spontaneous rate (HSR). The cube of calcium concentration is proportional to the release probability of a transmitter vesicle,

$$k(t) = z \left([Ca^{2+}]^3(t) \right), \quad (11)$$

where z is a constant for converting calcium concentration to release rate.

The IHC-synapse complex contained three stores of vesicles: The immediate (presynaptic) store with $q(t)$ vesicles, the synaptic cleft with $c(t)$ vesicles, and the reprocessing store with $w(t)$ vesicles. $k(t)$, previously computed, gives the vesicle transfer rate from the

immediate store to the synaptic cleft. Treating the transmitter as a continuous substance allows for the quantities to be tracked with

$$\frac{dq(t)}{dt} = N(w(t), x) + N([M - q(t), y]) - N(q(t), k(t)), \quad (12)$$

$$\frac{dc(t)}{dt} = N(q(t), k(t)) - lc(t) - rc(t), \quad (13)$$

and,

$$\frac{dw(t)}{dt} = rc(t) - N(w(t), x), \quad (14)$$

where l is the rate of neurotransmitter loss in the cleft, r is the rate of transfer of remaining neurotransmitter in the cleft to the reprocessing store, x is the rate of transfer of vesicles after repackaging to the immediate store from the reprocessing store, and M is the maximum vesicle holding capacity in the immediate store. The term $y[M - q(t)]$ describes the rate at which new transmitter vesicles replenish the immediate store. The function $N(n, \rho)$ describes the number of vesicles released in a time interval where ρ is the release rate, and n is the number of vesicles, each with a release probability of ρdt at timestep dt . $N(n, \rho)$ therefore outputs the release probability from the IHCs.

SGN Fiber Model

This model uses the NEURON simulator (Version 8.2) developed by Yale University and Duke University (Hines and Carnevale, 2001). In this study, the NEURON simulator was used to make a compartmental model of type I SGN peripheral axons (SGN fibers). Each fiber contained an unmyelinated segment with length L_u , a heminode with length L_h , and five myelin sheaths. For the purpose of this study, we only focused on changing the unmyelinated segment and kept the heminode length consistent in all trials. Each compartment was characterized by its specific capacitance (C_m) and specific membrane resistance (R_m) to describe passive membrane

properties. As this study uses a rodent model, to match the neural conduction velocity of the rodent auditory nerve, cytoplasmic resistance (R_a) was specifically chosen to maintain a 3-5m/s action potential speed (Tagoe et al., 2014; Mino et al., 2004). Channel dynamics parameters from Mino et al. (2004) were used with the exception of the stochastic channels which were converted to deterministic channels for simplicity. Simulations were run at 37°C. Potassium (E_K) and sodium ions (E_{Na}) were given values of 66mV and -88mV respectively, and the resting potential (E_{Rest}) was set to -78mV.

Each SGN fiber's transmembrane potential (V_m) was determined as a function of time t and space x ,

$$-\frac{\partial^2 V_m(x,t)}{R_a \partial x^2} + C_m \frac{\partial V_m(x,t)}{\partial t} + \frac{V_m(x,t) - E_{Rest}}{R_m} + I_{ion}(x, t) = I_{app}(x, t), \quad (15)$$

where $I_{ion}(x, t)$ is the ionic current and $I_{app}(x, t)$ is the applied current with respect to space x and time t .

Ionic current $I_{ion}(x, t)$ is calculated as a sum of the two ion currents, $I_{Na}(x, t)$ and $I_K(x, t)$:

$$I_{ion}(x, t) = I_{Na}(x, t) + I_K(x, t) \quad (16)$$

where

$$I_{Na}(x, t) = g_{Na}(m(t))^3 h(t) (V_m(x, t) - E_{Na}) \quad (17)$$

and

$$I_K(x, t) = g_{Na}(n(t))^4 (V_m(x, t) - E_k), \quad (18)$$

where g_{Na} and g_K are the maximal sodium and potassium conductances and $m(t)$, $n(t)$, and $h(t)$ are gating variables. From Mino et al. (2004), the gating variables are defined by functions $\alpha_i(V_m)$ and $\beta_i(V_m)$, where i is a placeholder variable for each of m, n, and h, as

$$\frac{di}{dt} = \alpha_i(V_m)(1 - i) - \beta_i(V_m)i \quad (19)$$

where,

$$\alpha_m(V_m) = \frac{1.872(V_m + 52.59)}{1 - e^{\frac{(V_m + 52.59)}{6.06}}} \quad (20)$$

$$\beta_m(V_m) = \frac{-3.973(V_m + 57)}{1 - e^{\frac{(V_m + 57)}{9.41}}} \quad (21)$$

$$\alpha_h(V_m) = \frac{-0.549(V_m + 105.74)}{1 - e^{\frac{(V_m + 105.74)}{9.06}}} \quad (22)$$

$$\beta_m(V_m) = \frac{-3.973(V_m + 22.57)}{1 + e^{\frac{-(V_m + 22)}{12.5}}} \quad (23)$$

$$\alpha_n(V_m) = \frac{0.129(V_m + 43)}{1 - e^{\frac{-(V_m + 43)}{10}}} \quad (24)$$

and

$$\beta_n(V_m) = \frac{-0.324(V_m + 68)}{1 - e^{\frac{-(V_m + 68)}{10}}}. \quad (25)$$

Generating AN Spike Times

Using the NEURON simulation, we were able to input the AN spike probabilities obtained from the Meddis model into a modified model (from Budak et al., 2021) to implement myelinopathy to the SGN fibers and determine spike times. This model determines the release times from inner hair cells based on the input release probabilities and generates spike times of each corresponding AN. The input contains probability data from the 21 channels previously

defined for each of the high (HT), medium (MT), and low threshold (LT) channels, resulting in 63 channels total. 100 fibers were then established for each of the 63 channels. Next, L_u and L_h values were assigned randomly between given bounds for each fiber. Since this study focused solely on the unmyelinated segment, L_u ranges were varied from no myelinopathy [10 μM , 10 μM] to random myelinopathy [10 μM , 20 μM], and L_h values were a consistent 1 μM . Release times were then determined. A counter was implemented to count action potentials at the heminode with a threshold of 10 μV . Synaptic currents from IHCs were then initialized with rise and decay time constants of 0.1 and 0.3 respectively with a reversal potential at 0mV (Budak et al., 2021). The previously determined L_u and L_h to the auditory fibers and channel conductance at the heminode was modified according to L_h with

$$g_K^{max} = \frac{0.225}{L_h} \quad (26)$$

and

$$g_{Na}^{max} = \frac{0.1812}{L_h} \quad (27)$$

where g_K^{max} and g_{Na}^{max} are the maximal potassium and sodium conductances respectively (Budak et al., 2021). Synaptic currents at release times were then found. Finally, the SGN fiber model NEURON simulation previously described was implemented to find AN spike times. This process was repeated for 3 trials and averaged to give the final spike times.

Developing Convolution for Compound Action Potential Response

To develop CAPs to represent the cumulative response of all SGN fibers in our simulation, spikes were convolved using the unitary response $U(t)$ described in Bourien et al. (2014; cited in Budak et al., 2021),

$$U(t) = \begin{cases} A \times e^{-k(t-0.288)} \times \sin(2\pi f(t - 0.288)) & \text{for } -0.215 \leq t \leq 2.785 \\ 0 & \text{otherwise} \end{cases} \quad (28)$$

where $A = 0.16\mu\text{V}$, $k = 1.44\text{ms}^{-1}$, $f = 0.994\text{ms}^{-1}$ and t is time.

Three populations were generated and averaged to construct an average CAP with error.

Three characteristic values of the CAPs were measured: delay (d), peak amplitude (a), and width (w),

$$d = t_{peak} - t_{start} \quad (29)$$

$$a = |p - b| \quad (30)$$

and,

$$w = 2(t_{peak} - t_w), \quad (31)$$

where t_{start} is the time of the onset of the sound signal, t_{peak} is the time at the peak (minimum) voltage, b is the baseline voltage calculated by averaging the convolution for .5ms before the sound onset, p is the peak (minimum) voltage, and t_w is the time at which the CAP is at $\frac{a}{2}\mu\text{V}$. A schematic of these calculations is shown in Figure 2.

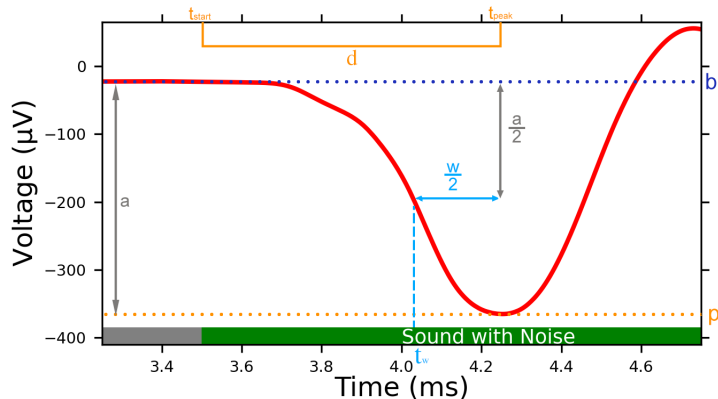


Figure 2: CAP measurements. The first peak after the introduction of noise is defined as the CAP. This is where delay, width, and amplitude are calculated to.

Results and Discussion

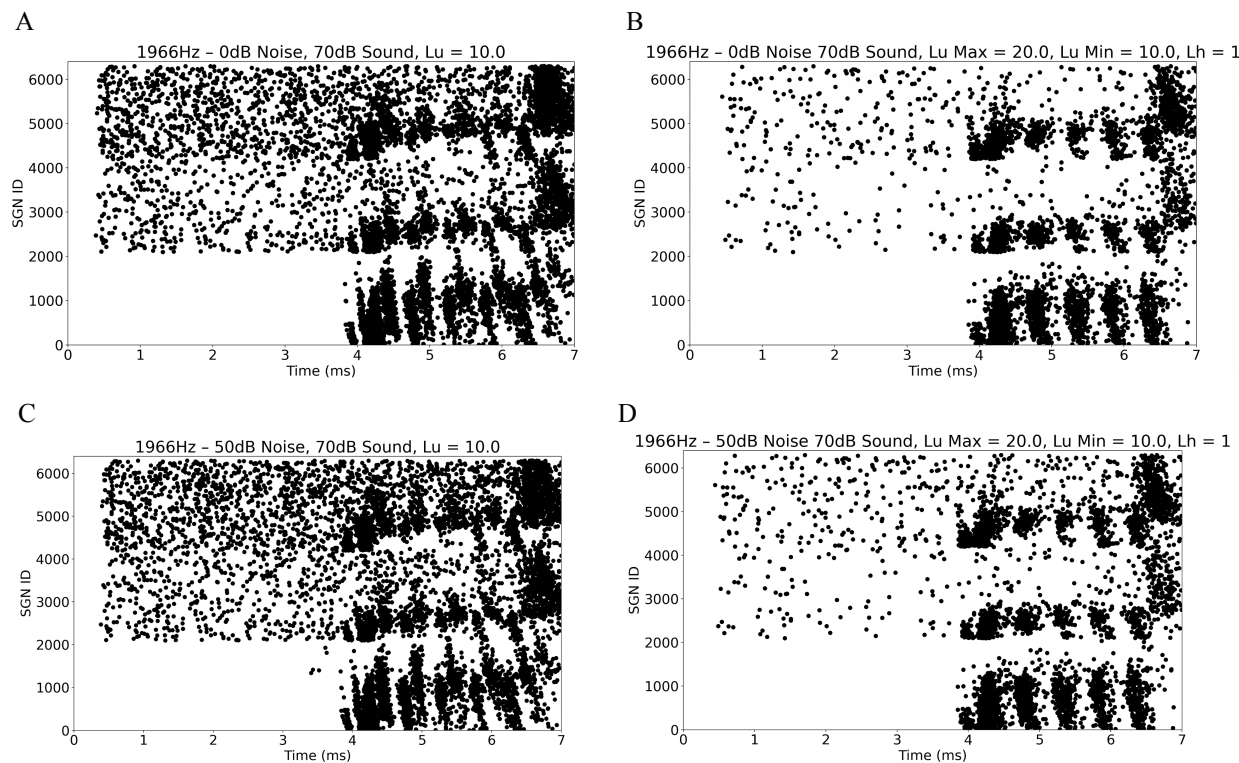
In this study we investigated the “cocktail-party effect” by implementing white noise over an intended sound signal representing human speech and recording type I SGN population activation patterns. We simulated environments of varying volume by adjusting the sound pressure level (dB SPL) of the background noise (between 0dB and 70dB) as well as the sound signal (between 30dB and 70dB). Sound and noise relationships can be described as sound-to-noise ratios (SNRs) as described in eq. 1. For clarity, a high SNR (>1) implies the sound signal SPL is greater than that of the noise signal, a moderate SNR ($=1$) implies the sound signal SPL is equal to that of the noise signal, and a low SNR (<1) implies the sound signal SPL is less than that of the noise signal. A clean sound signal is the sound signal alone with no noise input (or a 0dB SPL noise signal).

To mimic human speech, we chose three frequencies between 1kHz and 8kHz. Although typical human speech resides mostly between 500Hz-4kHz, we chose to go slightly beyond the upper bound because normal audiometric thresholds tend to allow for hearing up to 20kHz (Salmon et al., 2023). These parameters were simulated with normal myelination of the initial unmyelinated segment L_u ($10\mu\text{M}$) and random myelinopathy of the unmyelinated segment L_u ($10\text{-}20\mu\text{M}$) for all fibers of all thresholds (LT, MT, and HT). Results will be investigated with respect to frequency and will conclude with a comparison between the effects of the varying frequencies.

Effects of myelinopathy on SGN response to AWGN sound

The frequencies used in this study were specifically chosen to be spread relatively evenly between 1kHz and 8kHz, but also to be exactly the best frequency (BF; generated by the Greenwood function) of one of the channels. This range is well within the normal human audible

spectrum of 20Hz-20kHz, allowing for us to eliminate the possibility of boundary cases or effects. Sound levels were defined with the intention of simulating different conversational settings. We define a few analogies for understanding the sound levels chosen: 30dB – a soft whisper, 50dB – a normal conversation, 70dB – a washing machine (CDC, 2022). We chose not to go above 70dB as any noise beyond this level is considered potentially damaging and would overpower any typical conversational volume, defeating the purpose of the “cocktail-party effect.” Spiking during 0dB noise may seem counterintuitive, but is a product of spontaneous firing previously described in the methodology. In trials exhibiting myelinopathy, random L_u values between 10 and 20 μ m were assigned to extend the unmyelinated region in turn moving the heminode further from the IHC synapse (Budak et al., 2021). The effects of myelinopathy are present in Figure 2B with significant losses in spike density both in spontaneous and responsive firing.



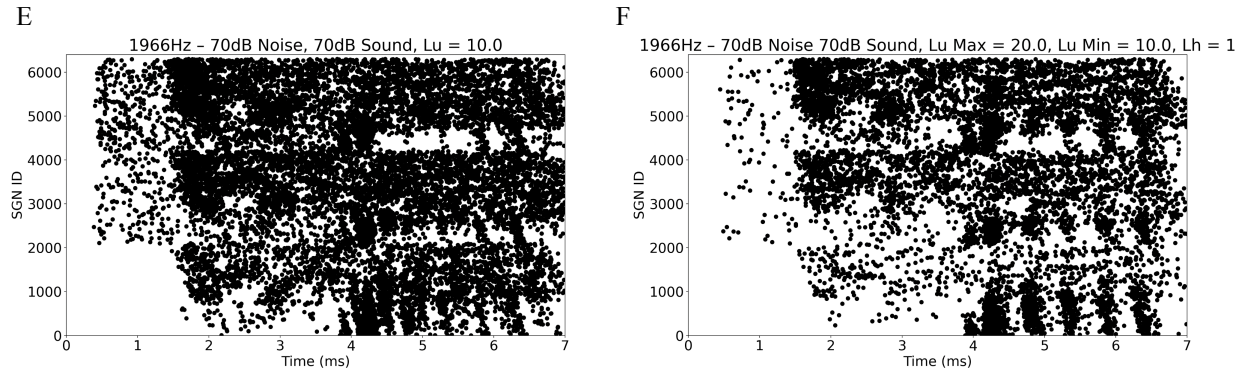


Figure 3: SGN spike times for 1966Hz, 70dB sound. Plots contain data from 6300 SGN fibers. SGNs 1-2100 are HT, 2101-4200 are MT, and 4201-6300 are LT. Fibers within their threshold ranges are organized by BF with the lowest BF at the bottom of these ranges and the highest BF at the top. (A) has normal myelination with the heminode sitting $10\mu\text{m}$ from the IHC-SGN synapse ($L_u = 10\mu\text{m}$) while (B) has random myelinopathy of the unmyelinated segment leaving the heminode between 10 and $20\mu\text{m}$ from the IHC-SGN synapse ($10\mu\text{m} \leq L_u \leq 20\mu\text{m}$). These values were calculated using the SGN fiber model described previously with no noisy signal. (C,D) and (E,F) show the effect of the implemented noisy signal (50dB and 70dB respectively) maintaining all other parameters.

Figures 3C, 3D, 3E, and 3F show increased spike density in the presence of white noise which is to be expected. However, there are similarities present between the SGN spike patterns with and without noise due to the greater sound SPL (70dB) compared to the noise SPL (50dB). These similarities can also be seen in the 70dB Adding white noise also appears to increase density more for the cases of normal myelination (3A and 3C). Figures 3E and 3F are responding both to the AWGN as well as the sound signal. This is apparent from the response at the top of each threshold range, indicating responses to high frequencies. White noise can be thought of as analogous to high frequency sound, so this response at the high BF fibers checks out. Although these results seem contradictory to our hypothesis, we can see the impact of white noise on the HHL in Figure 4.

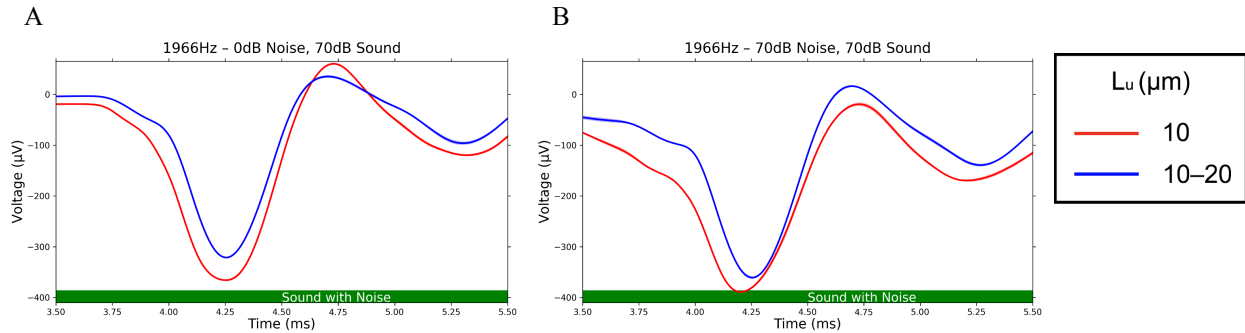
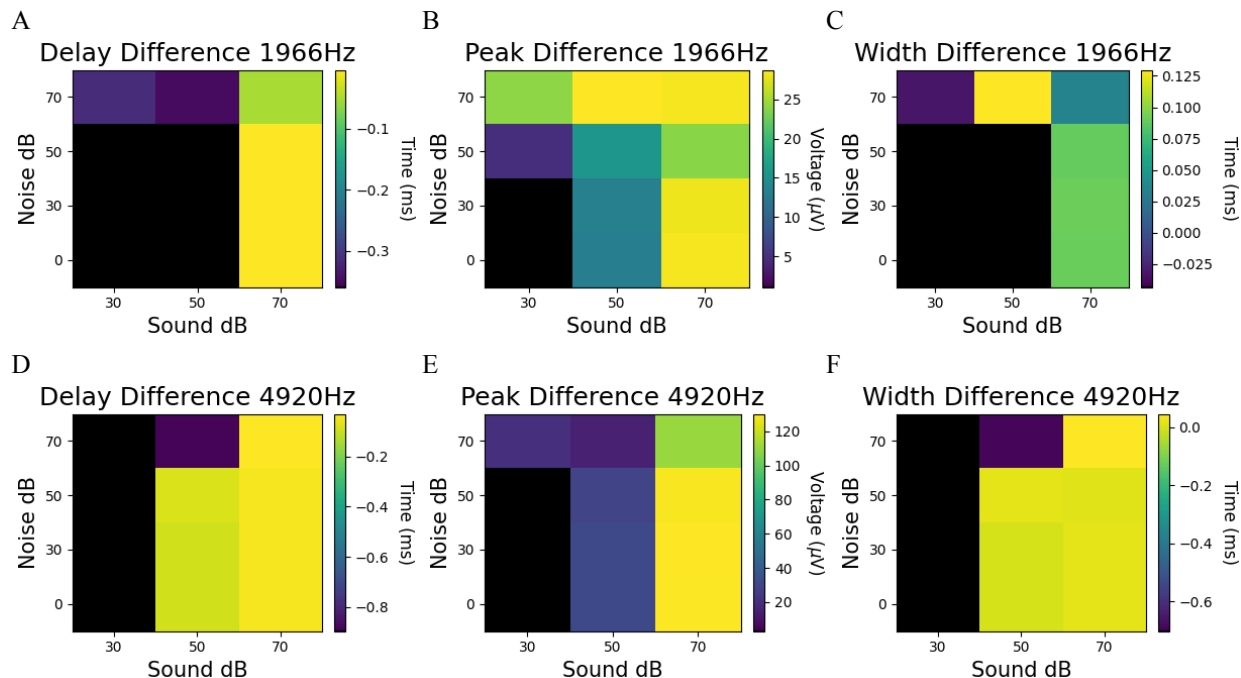


Figure 4: CAPs for 70dB 1966Hz sound signal with (A) 0dB noise and (B) 70dB noise. The red curves have normal myelination ($10\mu\text{m} = L_u$) and the blue curves have random myelinopathy of the unmyelinated segment ($10\mu\text{m} \leq L_u \leq 20\mu\text{m}$).

In the presence of the 70dB noise, both the normal and HHL CAPs reached lower voltages as predicted by the raster plots Figures 3E and 3F. The minimum voltage alone, however, can not determine the best response. Looking at the difference in delay time (t_{peak}) between the normal and HHL SGN CAPs, we see an increase in latency with the introduction of background noise. The differences between normal and HHL SGN unitary responses are displayed in Figure 5 for all frequencies.



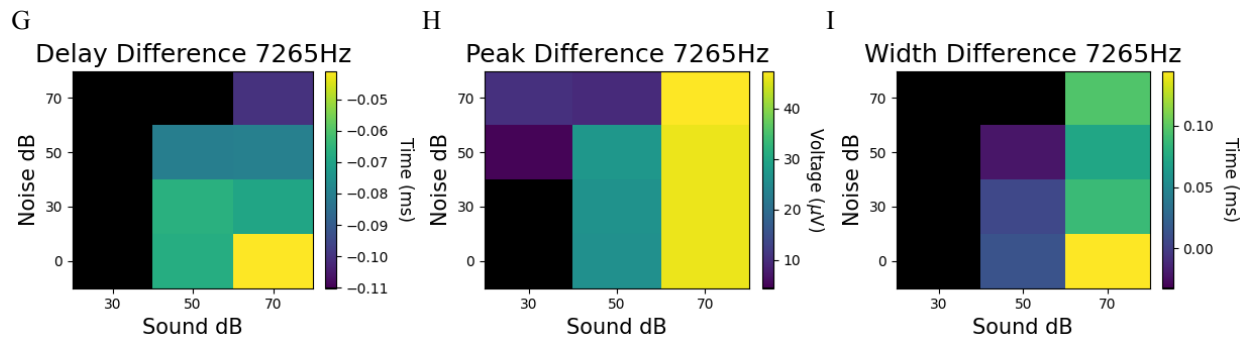


Figure 5: CAP data for all frequencies. Differences were calculated by subtracting the HHL value from the normal value for each of the three trials run, then averaging the differences calculated. Black squares indicate no CAP response was detected. This occurs with respect to the baseline (*b*) described in the methods.

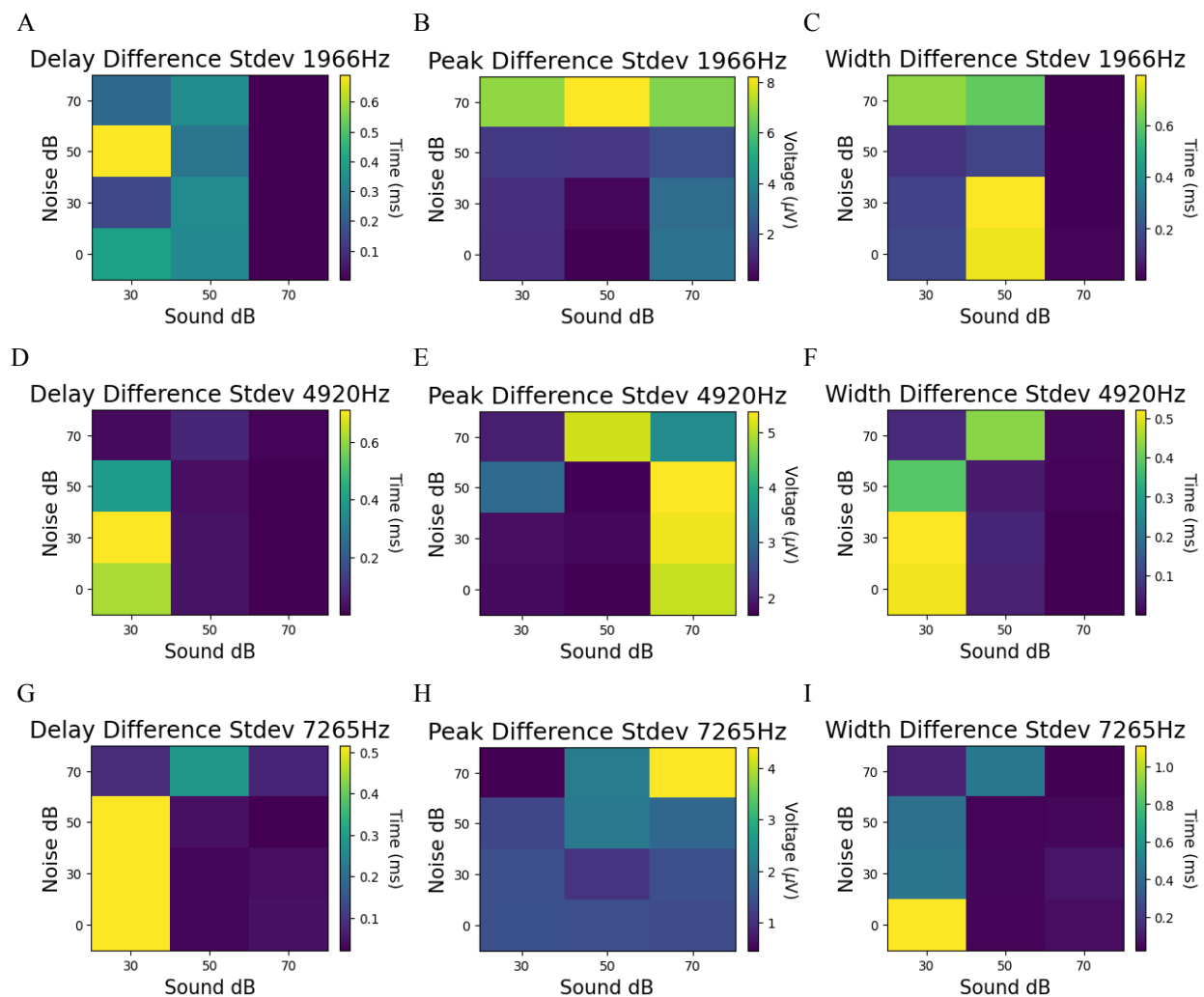


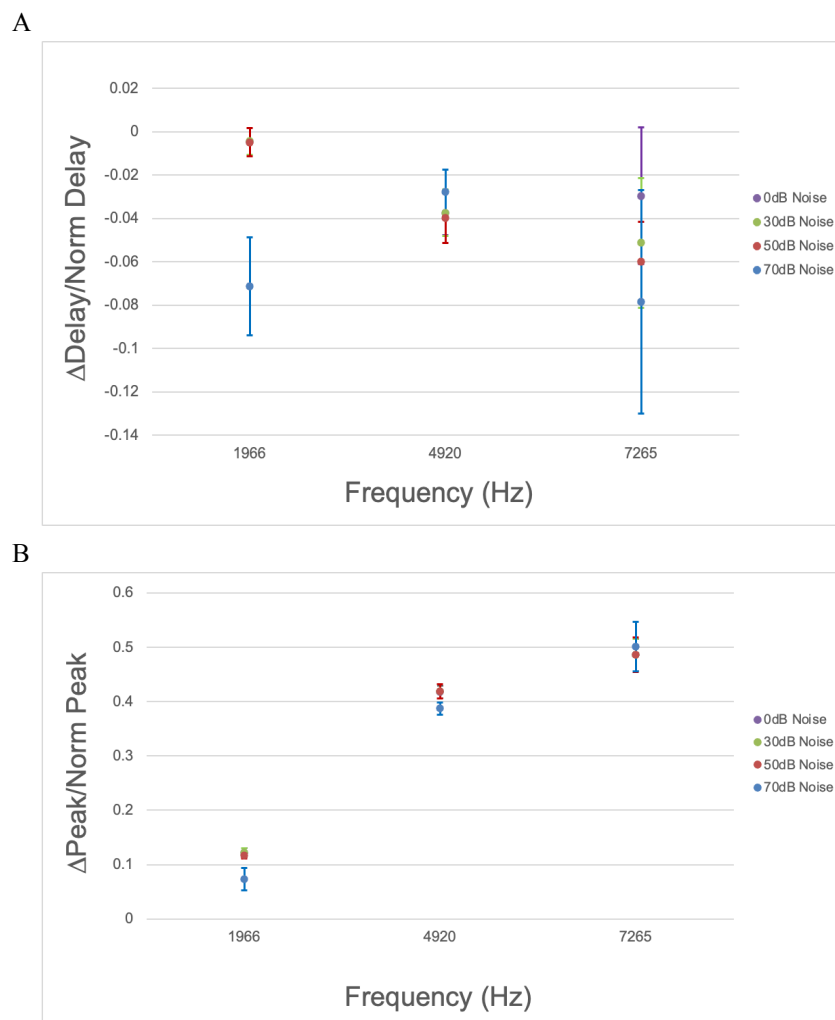
Figure 6: Standard deviations for CAP data. Standard deviations were calculated using the differences from the three trials. High standard deviations in delay and width indicate no CAP was detected.

As shown in the heatmaps, the effects of myelinopathy of the unmyelinated segment are exacerbated as the noise stimulus increases. Blacked-out cells on the heatmaps were omitted as no CAPs were detected and the model was in turn outputting default “maximum” widths and latencies spanning the entire simulation. This can be seen in Figure 6 where there are large standard deviations, indicating inconsistent measurements. Figures 5A and 5G display that the difference in delay decreases as the noise level increases. Differences are calculated by subtracting the HHL delay (d_{HHL}) from the normal delay (d_{norm}), so negative values imply $d_{HHL} > d_{norm}$. This aligns with our initial hypothesis that increased noise increases latency of SGN response. Peak difference results do not appear as linear as delay results (Figures 5B, 5E, and 5H). The greatest differences in peak amplitude occur at 70dB sound while the smallest differences occur at 30dB sound implying the effects of myelinopathy on signal strength may not be linear. Peak differences for 1966Hz simulations at 70dB noise are large indicating possible overpowering of the signal by the noise stimulus. This differs from the other frequencies indicating there may be a relationship between noise stimulus and the frequency of sound with respect to SGN activation.

We initially hypothesized that the CAP widths of the HHL SGN fibers would be greater than that of the normal SGN fibers, inline with the results found in Budak et al., (2021). However, we see in Figure 5 that this only holds true for the 4920Hz sound signal. This may indicate CAP width is frequency and noise dependent, adding on to the myelinopathy dependency already determined.

Comparison of frequency impact on SGN activation patterns

As seen in the previous section, there are implications that there may be relationships between frequency and SGN activation patterns when considering differences in myelin structure. CAP results were compared with respect to frequency by comparing the ratio of parameter difference (Δ Delay, Δ Peak, Δ Width) by the parameter's normal values with $L_u = 10\mu\text{m}$ (Norm Delay, Norm Peak, Norm Width) with a sound signal of 70dB SPL. Using peaks as an example for clarity, $\frac{\Delta \text{peak}}{\text{peak}_{\text{norm}}} \times 100$ gives the percentage decrease of the HHL peak amplitude from the normal peak amplitude.



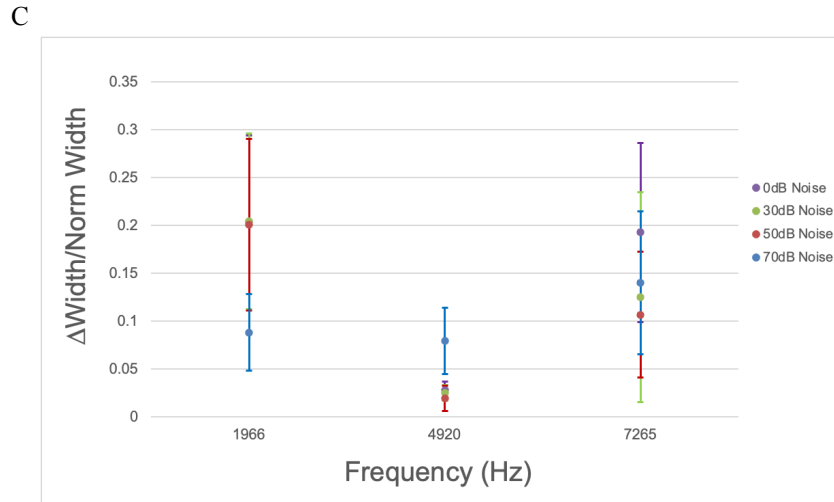


Figure 7: Delay, peak, and width values are compared by the frequency of the sound signal.
All measurements have a 70dB sound signal implemented, each color represents a noise SPL.

ΔDelay/norm Delay	0dB Noise	30dB Noise	50dB Noise	70dB Noise
1966Hz	-0.005±0.007	-0.004±0.007	-0.005±0.007	-0.071±0.025
4920Hz	-0.038±0.012	-0.037±0.012	-0.040±0.013	-0.028±0.012
7265Hz	-0.030±0.036	-0.051±0.034	-0.060±0.021	-0.078±0.058

Table 1: Means with 95% confidence intervals of Figure 7A. All simulations ran with a 70dB sound signal.

ΔPeak/norm Peak	0dB Noise	30dB Noise	50dB Noise	70dB Noise
1966Hz	0.122±0.009	0.123±0.008	0.117±0.006	0.073±0.021
4920Hz	0.417±0.011	0.419±0.013	0.418±0.013	0.387±0.011
7265Hz	0.486±0.029	0.486±0.029	0.487±0.032	0.501±0.045

Table 2: Means with 95% confidence intervals of Figure 7B. All simulations ran with a 70dB sound signal.

ΔWidth/norm Width	0dB Noise	30dB Noise	50dB Noise	70dB Noise
1966Hz	0.203±0.103	0.204±0.104	0.201±0.101	0.088±0.045
4920Hz	0.027±0.010	0.025±0.009	0.019±0.015	0.079±0.039
7265Hz	0.193±0.106	0.125±0.124	0.107±0.074	0.140±0.085

Table 3: Means with 95% confidence intervals of Figure 7C. All simulations ran with a 70dB sound signal.

Results showed the ratio of difference in peak amplitude to the normal peak amplitude increased with increasing frequency for all noise levels (Figure 7B). This implies the normal and HHL CAP peak amplitudes deviate greater as frequency increases. Delay ratios (Figure 7A) do not seem to have an apparent pattern, however it should be noted that all ratios appeared to converge at the moderate frequency (4920Hz) and diverge at the low and high frequencies. The width ratios (Figure 7C) all follow a similar pattern of decreasing as they approach the moderate frequency.

For all ratio comparisons, 0dB, 30dB, and 50dB noise simulations generally followed similar trends with some deviation at the highest frequency. This could be due to plotting responses to noise with a 70dB sound signal; the sound signal could be overpowering the background noise. This can be seen especially in Tables 1, 2, and 3 for the 0dB and 30dB noise where means and confidence intervals were nearly identical.

These findings give insight into the effects of hidden hearing loss in the “cocktail-party problem” and pave the way for future research in understanding the effects of myelinopathy and type I SGN firing patterns in noisy environments.

Limitations

Despite our findings, there are limitations that must be acknowledged. First, ideally we would have liked to run more than three trials per case, but runtimes and computing power were uncontrollable limitations in the scheme of this study. We would have preferred to run 50 trials (as done in Budak et al., 2021) to reduce error. We would have also liked to test more sound levels and degrees of myelinopathy to generate more understanding of the effects of white noise on those suffering from HHL. In the cases containing the highest frequency tested (7265Hz), deviations such as those seen in Figure 7 may have occurred due to the similarities the high

frequency shares in shape with pure white noise. It is also worth noting that 30dB sound did not generate much of an SGN response and might be too quiet to test at these high frequencies.

Future Research

To continue this experiment, we want to follow the protocol of Budak et al., (2022) to estimate sound localization and MSO responses with implemented white noise. We would also like to implement synaptopathy to determine the root cause of the cocktail-party effect.

References

- Bourien, J., Tang, Y., Batrel, C., Huet, A., Lenoir, M., Ladrech, S., Desmadryl, G., Nouvian, R., Puel, J. L., & Wang, J. (2014). Contribution of auditory nerve fibers to compound action potential of the auditory nerve. *Journal of neurophysiology*, 112(5), 1025–1039.
<https://doi.org/10.1152/jn.00738.2013>
- Budak, M., Grosh, K., Sasmal, A., Corfas, G., Zochowski, M., & Booth, V. (2021). Contrasting mechanisms for hidden hearing loss: Synaptopathy vs myelin defects. *PLOS Computational Biology*, 17(1). <https://doi.org/10.1371/journal.pcbi.1008499>
- Budak, M., Roberts, M. T., Grosh, K., Corfas, G., Booth, V., & Zochowski, M. (2022). Binaural processing deficits due to synaptopathy and myelin defects. *Frontiers in Neural Circuits*, 16. <https://doi.org/10.3389/fncir.2022.856926>
- Centers for Disease Control and Prevention. (2022, November 8). What noises cause hearing loss? Centers for Disease Control and Prevention. Retrieved March 23, 2023, from https://www.cdc.gov/nceh/hearing_loss/what_noises_cause_hearing_loss.html
- Kohrman, D.C., Wan, G., Cassinotti, L., & Corfas, G. (2020). Hidden Hearing Loss: A Disorder with Multiple Etiologies and Mechanisms. *Cold Spring Harbor perspectives in medicine*, 10(1), a035493. <https://doi.org/10.1101/cshperspect.a035493>
- Greenwood, D. D. (1990). A cochlear frequency-position function for several species--29 years later. *The Journal of the Acoustical Society of America*, 87(6), 2592–2605.
<https://doi.org/10.1121/1.399052>
- Heffner, R.S., Heffner, H.E. (1992). Evolution of Sound Localization in Mammals. In: Webster, D.B., Popper, A.N., Fay, R.R. (eds) *The Evolutionary Biology of Hearing*. Springer, New York, NY. https://doi.org/10.1007/978-1-4612-2784-7_43
- Hines, M.L., Carnevale, N.T. NEURON: a tool for neuroscientists. Neuroscientist. 2001; 7(2):123–35. <https://doi.org/10.1177/107385840100700207> PMID: 11496923.
- Lopez-Poveda, E. A., & Meddis, R. (2001). A human nonlinear cochlear filterbank. The Journal of the Acoustical Society of America, 110(6), 3107–3118.
<https://doi.org/10.1121/1.1416197>

- Meddis, R. (2011). Matlab auditory periphery (MAP) – Model technical description. Retrieved from
https://github.com/rmeddis/MAP/blob/master/Documentation/MAP%201_14%20Model%20description.docx.
- Meddis, R. et al. (2013). A Computer Model of the Auditory Periphery and Its Application to the Study of Hearing. In: Moore, B., Patterson, R., Winter, I., Carlyon, R., Gockel, H. (eds) Basic Aspects of Hearing. Advances in Experimental Medicine and Biology, vol 787. Springer, New York, NY. https://doi.org/10.1007/978-1-4614-1590-9_2
- Mino, H., Rubinstein, J.T., Miller, C.A., Abbas, P.J. (2004). Effects of electrode-to-fiber distance on temporal neural response with electrical stimulation. *IEEE Trans Biomed Eng.* 51(1):13–20. <https://doi.org/10.1109/TBME.2003.820383> PMID: 14723489.
- Salmon, M.K., Brant, J., Hohman, M.H., et al. Audiogram Interpretation. [Updated 2023 Mar 1]. In: StatPearls [Internet]. Treasure Island (FL): StatPearls Publishing; 2023 Jan-. Available from: <https://www.ncbi.nlm.nih.gov/books/NBK578179/>
- Tagoe, T., Barker, M., Jones, A., Allcock, N., Hamann, M. (2014). Auditory nerve perinodal dysmyelination in noise-induced hearing loss. *J Neurosci.* 34(7):2684–8. <https://doi.org/10.1523/JNEUROSCI.3977-13>. PMID: 24523557; PubMed Central PMCID: PMC6802753.
- Wan, G., & Corfas, G. (2017). Transient auditory nerve demyelination as a new mechanism for hidden hearing loss. *Nature communications*, 8, 14487. <https://doi.org/10.1038/ncomms14487>

Acknowledgements

I would like to thank Michal Zochowski, Maral Budak, and Victoria Booth for their immense support and encouragement throughout the research and writing processes. I appreciate all of their help and time sacrifices they made in their busy schedules to help me achieve my goals. I greatly appreciate Maral's graciousness in allowing me to use and modify her model and her help in implementing my data into said model. I want to thank Michal especially for agreeing to advise me on my thesis and training me to work on these models throughout the course of the last two years. I would also like to thank my family for their unwavering support and advice throughout this journey.